

# Low-loss $\text{Ba}_{0.5}\text{Sr}_{0.5}\text{TiO}_3$ thin films by inverted cylindrical magnetron sputtering

E. J. Cukauskas,<sup>a)</sup> Steven W. Kirchoefer, and J. M. Pond

Naval Research Laboratory, Electronics Science and Technology Division, Washington, DC 20375

(Received 3 December 1999; accepted for publication 20 June 2000)

The structural and electrical characteristics of  $\text{Ba}_{0.5}\text{Sr}_{0.5}\text{TiO}_3$  (BST) thin films deposited by inverted cylindrical magnetron rf sputtering have been investigated. This unconventional sputter deposition technique consisting of a hollow cylindrical composite target of BST, high argon/oxygen gas pressure 53.2 Pa (400  $\mu\text{m}$ ), and 750 °C substrate temperature was employed for depositing low-loss BST thin films. The films were postannealed in a tube furnace at 780 °C for 8 h in flowing oxygen. Atomic-force microscopy revealed anisotropic grain growth with a columnar grain structure protruding from the surface with a 0.25  $\mu\text{m}$  grain size. X-ray diffractometry shows the films to be purely (*h*00) oriented for certain deposition parameters. The lattice parameter of the best film was slightly larger than that for bulk BST. Other deposition conditions yielded films having many of the BST powder peaks. Capacitance versus voltage characteristics have been measured from 50 MHz to 20 GHz. Device  $Q$  values  $>600$ , beyond the resolution of the device/measurement system, were realized with a 6.7% tunability at 10 GHz for the best films. [S0021-8979(00)01119-1]

## I. INTRODUCTION

Currently there is great interest in the development of high-quality ferroelectric thin films of  $\text{Ba}_{(1-x)}\text{Sr}_x\text{TiO}_3$  (BST) for applications in voltage-tunable microwave components and in dynamic random access memory computer memory elements.<sup>1,2</sup> BST forms a solid solution for all Ba/Sr metals fractions, making it ideally suitable for room-temperature ferroelectric device applications. Additionally, BST can easily be made by many standard thin-film deposition techniques, however, the properties of low-loss, low-leakage current, and a large change in dielectric constant ( $\epsilon_r$ ) with applied voltage (tunability) have not been fully attained. At issue for most deposition techniques is the ability to reproducibly grow thin-film BST which simultaneously has low loss and a practical tunability at room temperature. Of interest is the relationship between the electrical properties of loss and tuning to that of film morphology and the deposition parameters associated with the particular growth process. The transport of the BST constituents to the substrate can vary widely depending upon the growth process and may result in different microstructures and ferroelectric properties. In our previous work, we demonstrated that high-quality BST thin films can be grown by off-axis cosputtering of  $\text{BaTiO}_3$  and  $\text{SrTiO}_3$  to yield any Ba/Sr metals fraction from only two targets. The metals fraction was set by the relative power levels of the targets. This unique technique yielded specular films having device  $Q$  values exceeding the resolution of the device/measurement instrumentation.<sup>3</sup>

In this article, we report our initial results of the material and electrical characteristics of BST thin films sputter deposited by the unconventional technique of inverted cylindrical magnetron (ICM) rf sputtering. The ICM sputtering technique is capable of deposition rates greater than 1 Å/s, al-

lowing for rapid turn around for thin-film studies. The resulting films are single-phase BST whose orientation and electrical properties are strongly dependent on the deposition parameters. Interdigitated capacitors fabricated from the films had  $Q > 600$  with nearly 7% tuning for the best films.

## II. FILM GROWTH

Sputtering is an acceptable manufacturing process for the deposition of thin films for electronic devices and integrated circuits. Radio-frequency reactive sputtering is a proven and complex technique for the deposition of high-quality thin oxide films for electronics.<sup>4</sup> However, the sputter deposition of oxide films has the potential for film degradation by neutral and negative-ion bombardment of the growing film. For multication materials such as BST, this resputtering can lead to off-stoichiometric films and degradation of electrical properties. The use of high sputtering gas pressure, unconventional system geometries, or the use of composition-compensated targets are some ways to minimize these adverse effects. The ICM sputter gun is one such unconventional geometry and has proved highly successful for the deposition of stoichiometric thin films of the oxide superconductor  $\text{YBa}_2\text{Cu}_3\text{O}_7$ .<sup>5</sup>

In this investigation, we studied  $\text{Ba}_{0.5}\text{Sr}_{0.5}\text{TiO}_3$  films deposited by ICM rf sputtering of a composite  $\text{Ba}_{0.5}\text{Sr}_{0.5}\text{TiO}_3$  target of 99.9% purity. The films were deposited on 6.4-mm-square (100) MgO substrates. All of the BST films were deposited in an Ar/O<sub>2</sub> gas mixture set by individual mass-flow control valves. Unless otherwise stated, the sputtering pressure was maintained at 53.2 Pa (400  $\mu\text{m}$ ) and the gas mixture ranged from 2.5% to 100% oxygen. The deposition rate was first calibrated for the system geometry, pressure, and substrate temperature.

<sup>a)</sup>Electronic mail: cukauskas@estd.nrl.navy.mil

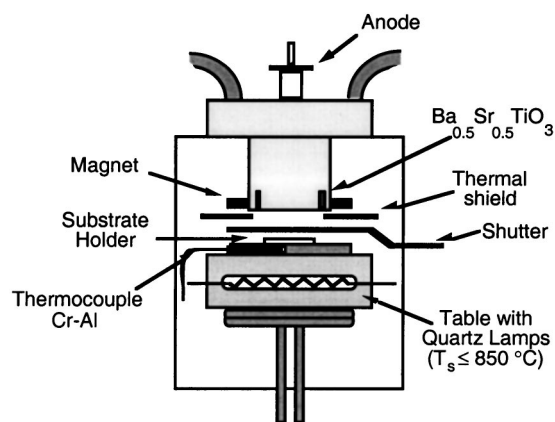


FIG. 1. Geometry of the ICM sputter gun and substrate table used to deposit BST thin films. The relative position of cathode, anode, and substrate serves to minimize resputtering the growing film.

The BST films were deposited on the MgO substrates heat sunk by silver paste onto a stainless-steel substrate holder. Figure 1 illustrates the ICM sputter gun and table geometry used for film growth. A copper water-cooled cathode houses the hollow cylindrical BST target surrounded by a ring magnet concentric with the target. A stainless-steel thermal shield is mounted very close to the gun to shield the magnet from the thermal radiation coming from the heated table. The anode is recessed in the hollow-cathode space and aids in collecting electrons and negative ions, thus minimizing resputtering the growing film. This geometry assures that the composition of the deposited thin film replicates that of the target.<sup>5</sup> Outside the deposition chamber, a copper ground wire is attached between the anode and the stainless-steel chamber. Alternatively, a dc bias voltage can be applied to the anode to alter the plasma characteristics in the cathode/anode space. The sputter gas enters the cathode region through the space surrounding the anode.

The BST films were deposited at a number of temperatures ranging from 550 to 800 °C. The substrate holder temperature was maintained by two quartz lamps, a type-K thermocouple and a temperature controller. The films were deposited at 135 W to a film thickness of 7000 Å. The resulting growth rate was approximately 0.41 Å/s. Although the growth rate is known to influence the material and electrical properties of thin films, it was not investigated in this work. The films were cooled to room temperature in 1 atm of oxygen before removing them from the deposition system. This was followed by annealing the films in 1 atm of flowing oxygen at a temperature of 780 °C for 8 h in a tube furnace. The cool down in oxygen and postannealing were done to reduce any oxygen deficiency in the films.<sup>5,6</sup> It is known that the oxygen vacancy density is decreased by a postanneal in oxygen.<sup>6</sup>

### III. MORPHOLOGY CHARACTERIZATION

The kinematics of film growth can lead to a diversity of morphological features which impact the electrical properties of thin-film BST. Surface features can be investigated by atomic-force microscopy (AFM) and the grain structure by

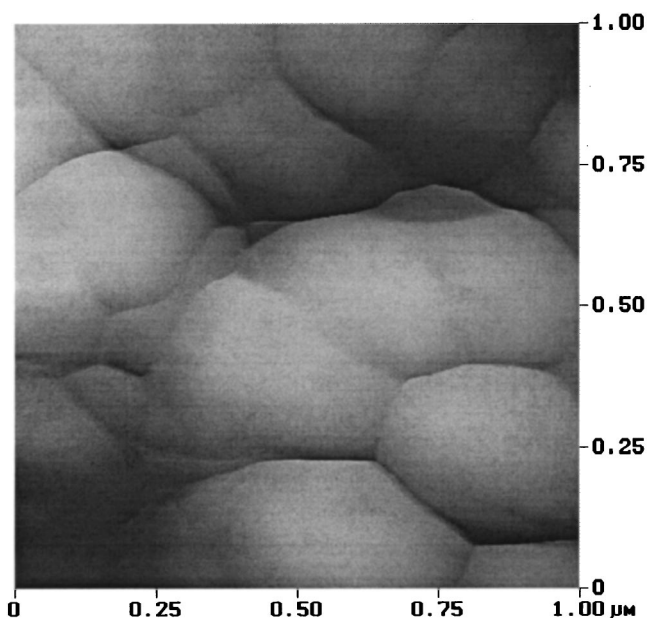


FIG. 2. Surface view of a 1  $\mu\text{m}^2$  area of a low-loss BST film deposited at 750 °C substrate temperature. Visible are the 0.25  $\mu\text{m}$  grains.

x-ray diffractometry. We used AFM imaging to study surface roughness and grain size of the ICM-sputtered BST while the lattice parameter and grain orientation were determined by x-ray diffractometry.

#### A. Surface morphology

The film morphology was investigated using a Digital Instruments Nanoscope model IIIa. The surface roughness was determined for a number of films from the AFM images and the instrument's data analysis software. The root-mean-square (rms) surface roughness is defined by

$$\text{rms} = \left\{ \frac{1}{N} \sum_{i=1}^N (Z_i - Z_{\text{avg}})^2 \right\}^{1/2}, \quad (1)$$

where  $Z_i$  is the height of the  $i$ th point and  $Z_{\text{avg}}$  is the arithmetic average height within the measurement area. The rms surface roughness is a measure of the peak-to-peak distance between the grain peaks and underlying continuous film. Figure 2 illustrates the surface of a BST film deposited at a substrate temperature of 750 °C. This film has a surface roughness of approximately 70 nm. An oblique angle view of the surface shows columnar grains protruding above a continuous film. Assuming the  $c$  axis is taken as being perpendicular to the substrate, the growth rate along the  $c$  axis is greater than that in the plane of the substrate. The growth rate is nearly isotropic below 550 °C and becomes progressively more anisotropic at higher substrate temperatures. The rms surface roughness is a measure of this growth anisotropy.

Substrate temperature is known to affect the morphology of oxide films grown by ICM sputtering.<sup>5</sup> The effect of the other deposition parameters on this growth rate anisotropy is currently under investigation. Preliminary results show a strong dependence of surface roughness on the gas sputtering parameters. A closer examination of the grain structure in

Fig. 2 shows the film consisting of coupled grains on the submicron scale with a typical grain size of  $0.25 \mu\text{m}$ . The image illustrates that the  $0.25 \mu\text{m}$  grains coalesce and form larger grains having barely visible, yet still discernible, grain boundaries. These larger grains grow rapidly perpendicular to the plane of the substrate, which results in the large roughness for films made at the higher substrate temperatures.

## B. X-ray diffractometry

The crystal structure was determined for a select number of films from x-ray diffraction scans taken with an automated independent theta-two-theta diffractometer. Scans in two-theta were taken from  $20^\circ$  to  $110^\circ$ . In general, the x-ray peak spectra were that of mixed textured BST films dominated mostly by the ( $h00$ ) reflections and substrate peaks. However, for certain deposition parameters the ( $h00$ ) peaks were absent. The spectrum of peak positions for each film was analyzed using the Nelson–Riley  $\cos^2 \theta / \sin^2 \theta + \cos^2 \theta / \theta$  error correction and a linear least-squares fit in calculating the lattice parameter. The crystal structure of the films was studied in order to gain insight in establishing the optimum deposition conditions for growing the proper phase and orientation of the BST films. The lattice parameter for as-deposited films showed little or no change after postannealing. The dielectric constant of the ferroelectric films is influenced by the grain structure and the quality of the material throughout the volume of the film. Furthermore, the Curie temperature of BST is directly related to the unit-cell volume or lattice parameter.<sup>7</sup>

We investigated the crystal structure of the BST films made at different substrate temperatures, different Ar/O<sub>2</sub> mixtures, and for several substrate-to-target spacings. The structure was studied for films deposited at substrate temperatures ranging from  $550$  to  $800^\circ\text{C}$ , Ar/O<sub>2</sub> gas mixture ranging from 100% argon to 100% oxygen, and for substrate-to-target ground shield distance of zero to  $13.5$  mm. Films deposited at  $550^\circ\text{C}$  were mixed textured and became more ( $h00$ ) oriented for higher substrate temperatures. Additionally, the film texture was also influenced by the sputter gas composition.

The BST structure was not observed for films made at very low oxygen concentration (<5%). As the percent of oxygen in the sputter gas was increased above 5%, the BST structure became dominated by the ( $h00$ ) orientation. BST deposited in 100% oxygen was predominantly ( $110$ ) oriented. The optimum Ar/O<sub>2</sub> sputter gas mixture was found to be approximately 85% oxygen, which resulted in large peak heights. The effect of the target-to-substrate spacing was investigated for this gas mixture. Films deposited at the minimum substrate-to-target spacing had mixed orientations and were characterized by low diffraction peak heights. For those films made at greater spacings, the diffraction scans showed greater peak heights and stronger ( $h00$ ) orientation. The most highly textured films were made at a spacing of  $8.6$  mm and were purely ( $h00$ ) oriented.

Figure 3 illustrates the x-ray diffraction scan for a BST film made with 85% oxygen and a  $750^\circ\text{C}$  substrate temperature. This is the same film whose AFM surface image is

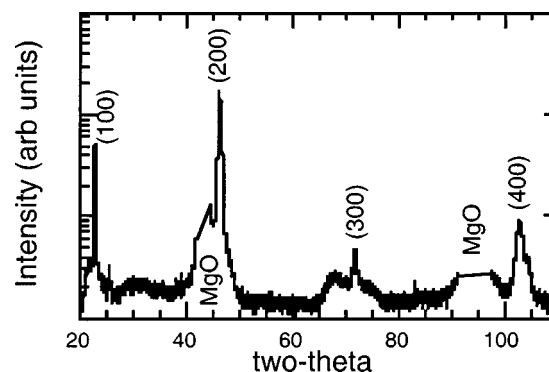


FIG. 3. X-ray scan of a BST thin film deposited at  $750^\circ\text{C}$  substrate temperature in a 85% oxygen/argon gas mixture. The substrates were positioned  $8.6$  mm below the gun thermal shield. The MgO substrate peaks were suppressed from the data.

illustrated in Fig. 2. The table was positioned  $8.6$  mm below the gun thermal shield. At greater spacing, the peak intensity fell off but the films were still purely ( $h00$ ) oriented. This orientation effect may result from the BST molecules remaining in the plasma for a greater number of mean-free-path lengths before condensing on the substrate, and thus increasing the probability for complete oxygenation and thermalization.

## IV. ELECTRICAL CHARACTERIZATION

The BST thin films were processed into arrays of interdigitated capacitors with a variety of device dimensions. Details of the processing can be found elsewhere.<sup>8</sup> The capacitors were characterized using a microwave probe station in conjunction with a HP 8510C vector network analyzer. Room-temperature reflection measurements ( $S_{11}$ ) were made over a frequency range from  $50$  MHz to  $20$  GHz. An external biasing network was used to apply a voltage from  $-40$  to  $+40$  V, and back to  $-40$  V, in  $5$  V increments. The  $S_{11}$  measurement data were analyzed using a parallel resistor–capacitor circuit model for determining the device  $Q$  and the capacitance. To obtain the relative dielectric constant and loss tangent of a film, a conformal-mapping, partial-capacitance approach similar to that described by Gevorgian *et al.* has been implemented.<sup>9</sup> Although only applicable at frequencies which are sufficiently low that the device is electrically small, the small dimensions of the interdigitated capacitor allow this technique to be applied at frequencies up to at least  $10$  GHz or higher depending on the total relative dielectric constant. Using this approach, the relative dielectric constant of the ferroelectric thin film can be calculated given the geometry of the interdigitated capacitor, the thickness of the ferroelectric thin film, the thickness and dielectric constant of the substrate, and the measured capacitance.

### A. Microwave measurement results

Figure 4 illustrates the relative dielectric constant and loss tangent as a function of bias voltage measured at  $10$  GHz for a low-loss BST film. The film was deposited at a substrate temperature of  $750^\circ\text{C}$  and 85% oxygen in the sputter gas mixture. The AFM image and x-ray trace of this film

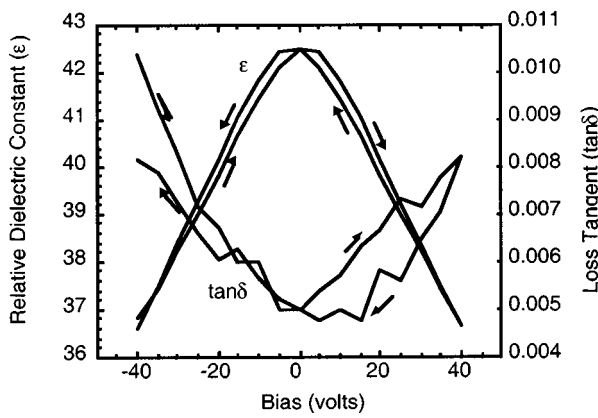


FIG. 4. Relative dielectric constant and loss tangent as a function of bias voltage measured at 10 GHz. The direction of the bias sweep is indicated by the arrows. The film was deposited on MgO at 750 °C in a 85% oxygen gas mixture. The film’s x-ray scan is illustrated in Fig. 3.

are illustrated in Figs. 2 and 3. Although the rms surface roughness of the film was 70 nm, it still had excellent electrical properties. Both the capacitance and loss exhibited little frequency dependence. However, note that the loss increases at higher bias. This may be attributed to parallel conduction along the many grain boundaries in these fine-grained films. The noise in the  $Q$  data at these high values is due to a loss of resolution inherent in this broadband measurement technique. The capacitance value and the relative dielectric constant are rather small, which we associate with the film’s small grains, operating in the paraelectric state, or that the film may be a relaxor-type ferroelectric.<sup>10–12</sup> Based on the lattice parameter determined from the x-ray scan illustrated in Fig. 3, the Curie temperature is estimated to be  $-20$  °C.<sup>7,11</sup> This places the room-temperature measurement  $40$  °C into the paraelectric region where reduced tuning and lower loss are expected. Note the hysteresis in the dielectric characteristic. This hysteresis can result from macroscopic regions of differing Curie temperatures and/or relaxor behavior.

A summary of the results for a select number of devices is listed in Table I. The fractional tuning is defined as  $[C(0) - C(40)]/C(0)$ , where  $C(0)$  and  $C(40)$  are the capacitance at 0 and 40 V, respectively. The figure of merit (FOM) listed in Table I is defined as the product of the average  $Q$  and the fractional tuning for the device. This allows for a sample-to-sample comparison encompassing both loss and tuning. The films deposited on substrates held at

$750$  °C had the best electrical properties. We found that films deposited in a gas mixture containing 85% oxygen had improved loss and tuning. In contrast, films made with only a few percent oxygen had both low  $Q$  and small tuning. This is consistent with the absence of the BST diffraction peaks in the x-ray diffraction scans for these films. The ICM sputter gun geometry is such that damage to the growing film from negative-ion bombardment is minimized. However there is an optimum target-to-substrate distance. We found that for a 8.6 mm distance between the gun thermal shield and substrate table resulted in very high  $Q$  and a reasonable tuning of nearly 7%. These results are summarized in Table I along with other relevant data.

### B. Curie temperature

Zhang *et al.* have shown that the Curie temperature of BST is determined by the unit-cell volume.<sup>7</sup> They observed this to be true for composition changes or induced film stress. Additionally, stress can be caused by oxygen deficiencies in perovskite and result in an enlarged lattice parameter.<sup>13</sup> The lattice parameter of BST is linearly dependent on composition over the entire range of Ba/Sr metals fractions. Davis and Rubin have related the Curie temperature of BST to composition.<sup>14</sup> Combining these results, we can calculate the Curie temperature as a function of lattice parameter for all BST compositions. For compositions where the unit cell is tetragonal, the cube root of the cell volume is used in place of the lattice parameter. An empirical relationship determined from a least-squares fit to the data of Davis and Rubin<sup>14</sup> is given by Eq. (2):

$$T_c = -13242 + 3344.4 * a_0, \tag{2}$$

where  $T_c$  is the Curie temperature in °C and  $a_0$  is the lattice parameter in Å. The relative dielectric constant ( $\epsilon$ ) is given by Eqs. (3) and (4) as a function of the constant ( $C$ ), the temperature ( $T$ ), and  $T_c$  for the ferroelectric and paraelectric state, respectively:

$$(\epsilon - 1)/C = 1/2 * (T_c - T), \quad T < T_c, \tag{3}$$

$$(\epsilon - 1)/C = 1/(T - T_c), \quad T > T_c. \tag{4}$$

Combining Eqs. (2), (3), and (4) and setting  $T = 20$  °C, for the measurement temperature yields the relationship between  $T_c$  and  $a_0$ . This relationship is plotted in Fig. 5 together with the measured dielectric constant for a number of our BST thin films. The solid lines, Eqs. (3) and (4), in Fig. 5 are not

TABLE I. Summary of properties for selected BST thin films.

| Sample No. | Table (mm) | $Q$  | Tuning (%) | FOM  | Curie $T$ (°C) | $\epsilon$ at 0 V | $a_0$ (Å) | Remarks   |
|------------|------------|------|------------|------|----------------|-------------------|-----------|---|
| 23         | 0          | >600 | 1          | >6   | -43            | 22.8              | 3.9466    | Low-intensity peaks                                       |
| 20         | 3.8        | 156  | 5.6        | 8.7  | -4.9           | 97                | 3.9580    | Strong-intensity peaks                                    |
| 22         | 8.6        | >600 | 6.7        | >40  | -19.6          | 41.6              | 3.9536    | High-intensity ( $h00$ )                                  |
| 27         | 13.3       | 107  | 0.68       | 0.73 | -97.5          | 10                | 3.9302    | Low-intensity ( $h00$ )                                   |
| 17         | 3.8        | 46   | 7.1        | 3.3  | 72.7           | 56.4              | 3.9812    | 100% O <sub>2</sub> , no ( $h00$ )                        |
| 43         | 8.6        | 85.5 | 1.71       | 1.46 | -55.03         | 105               | 3.9643    | High-intensity ( $h00$ )                                  |
| 55         | 8.6        | 26   | 2.59       | 0.67 | 253            | 49.4              | 4.0351    | High-intensity ( $h00$ ), Ar/O <sub>2</sub> at 50 $\mu$ m |

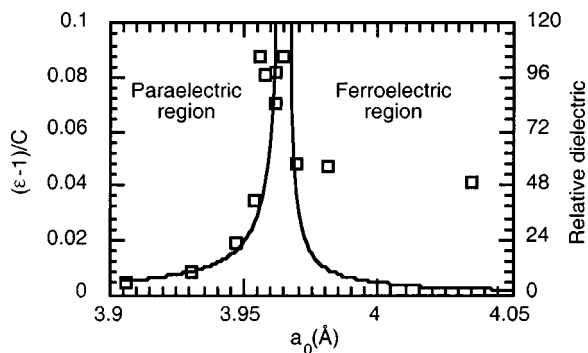


FIG. 5. Relative dielectric constant and the expected theoretical dependence on the lattice parameter of the BST thin films. Most of the films are in the paraelectric state at room temperature. The solid lines are not a fit to the data and show only the functional form.

a fit to the experimental data but show the expected dependence of the measured dielectric constant on the lattice parameter.

The lattice parameter for BST with  $x=0.5$  is  $3.9471 \text{ \AA}$  and has a Curie temperature of  $-41.3 \text{ }^\circ\text{C}$ . At room temperature, a BST film with these parameters is in the paraelectric state. A view of Fig. 5 shows most of the BST films are in the paraelectric state. However, many are far into the paraelectric region and some in the ferroelectric region. These results show that the dielectric properties of thin-film BST are strongly dependent on the lattice parameter. These films were deposited under a variety of deposition parameters and from the same stoichiometric  $x=0.5$  BST target. Those films having the greatest dielectric constant are clustered around a Curie temperature of  $0 \text{ }^\circ\text{C}$  or a lattice parameter of  $3.9595 \text{ \AA}$ . This corresponds to the composition  $\text{Ba}_{0.65}\text{Sr}_{0.35}\text{TiO}_3$  and is a good composition for developing optimum dielectric properties in BST thin films. At issue with thin-film BST is the origin of the lattice-parameter expansion or contraction in relation to stress and/or oxygen deficiencies. These deficiencies can contribute to loss through their influence on the Curie temperature.

### C. Loss in ICM-sputtered BST

Leakage currents and microwave loss mechanisms are areas of fundamental importance and are influenced by the deposition parameters used for BST film growth. Small-grained films have many grain boundaries and any low-resistivity material within the boundaries forms a parallel conduction path contributing to the measured dielectric loss. Additionally, the magnitude of the density of oxygen vacancies in BST contributes to the leakage current.<sup>6,15,16</sup> The expanded lattice parameter in many of our films is consistent with oxygen vacancies. Waser, Baiatu, and Hardtl have shown that fine-grained films have a lower resistance degradation rate than larger-grained films.<sup>17</sup> They attribute this to the grain boundaries acting as barriers to the migration of oxygen vacancies.

Researchers have also modeled the mechanisms of leakage current as due to thermionic emission over the Schottky barrier formed by the metal electrodes with BST and by tunneling currents through the depletion width at the Schottky

barrier.<sup>18,19</sup> For our interdigitated capacitor geometry, such Schottky effects should not be the major contribution to loss in our BST films. The finger gaps are of such great distance that any Schottky barrier effects would be very small in relation to the space-charge-limiting effects of electron injection into the insulating BST. In this case, the measured loss will originate primarily from the interior of the film with some contribution from the BST/air interface. However, the high- $Q$  values achieved in some of our films support the conclusion that they consist of well-oxygenated grains. For these films, the loss may still originate from any oxygen vacancies and parallel conduction along the grain boundaries. Furthermore, the increase in loss with dc bias for our interdigitated capacitors is compatible with the increase in leakage conduction with voltage observed by Kim and Park for their parallel-plate capacitors.<sup>20</sup>

### V. SUMMARY AND CONCLUSIONS

Thin films of BST with low loss have been deposited by unconventional ICM rf sputtering of a composite BST target on (100) MgO substrates held at elevated temperatures. The high sputtering gas pressure of  $53.2 \text{ Pa}$  and the ICM gun geometry served to minimize resputtering of the growing film. Postannealing the films in  $1 \text{ atm}$  of flowing oxygen at  $780 \text{ }^\circ\text{C}$  for  $8 \text{ h}$  was done to reduce defects, increase grain size, and help to reduce the number of oxygen vacancies. X-ray diffraction scans taken on the films indicate the BST structure is formed with an expanded lattice parameter. However, the oxygen postanneal had little effect on the lattice parameter of the as-deposited films. The crystallite orientation was strongly dependent on substrate temperature, gas composition, and the substrate-to-target distance. The films, which had a purely ( $h00$ ) crystallite orientation on the (100) MgO substrates, were positioned  $8.6 \text{ mm}$  below the gun ground shields during deposition. Substrates closer to the gun resulted in films having many of the BST powder peaks. Diffraction peak height increased with increasing deposition temperature. The surface roughness also increased with deposition temperature from specular (rms  $\sim 20 \text{ nm}$ ) at  $550 \text{ }^\circ\text{C}$  to visually rough (rms  $\sim 70 \text{ nm}$ ) at  $750 \text{ }^\circ\text{C}$ . The typical grain size was observed to be  $0.25 \text{ }\mu\text{m}$ . These submicron grains coalesce and form larger grains which grow as columnar-like spikes above the film surface. Films deposited with small amounts of oxygen ( $<5\%$ ) did not have the BST structure and had low  $Q$  and small ( $<1\%$ ) tuning. The best films with very low loss were deposited at  $750 \text{ }^\circ\text{C}$  and were purely ( $h00$ ) oriented. The electrical characteristics improved with increasing deposition temperature and were not degraded by the increasing surface roughness. Although low loss, oxygen vacancies and parallel conduction along the grain boundaries of the film are the mechanisms we believe are responsible for the measured loss in these films.

In conclusion, low-loss thin-film BST can be deposited by ICM sputtering from a  $\text{Ba}_{0.5}\text{Sr}_{0.5}\text{TiC}_3$  composite target. Films grown on MgO substrates held at high substrate temperature ( $750 \text{ }^\circ\text{C}$ ) have good dielectric properties and are strongly ( $h00$ ) orientated. This orientation is accompanied by large protruding ( $h00$ ) grains resulting in a rough film

surface. From this protruding grain morphology it is concluded that there is an anisotropy in the growth rate perpendicular to the plane of the substrate becoming greater with increasing substrate temperature. The sputter growth process produces films having fine ( $\sim 0.25 \mu\text{m}$ ) grains with barely discernible grain boundaries contributing to lower loss. From structural analysis of these BST films we conclude that the dielectric properties are strongly affected by the lattice parameter. Deviation of the lattice parameter is a result of film stress and/or oxygen vacancies. The Curie temperature, which is strongly influenced by the lattice parameter, determines the optimum operating temperature of the ferroelectric/paraelectric state of thin-film BST. From the correlation of the dielectric properties, lattice parameter, and Curie temperature, we conclude that the lattice parameter is a good measure of the expected dielectric properties of the film. From the peak in the dielectric constant versus the lattice parameter, we conclude that the composition  $\text{Ba}_{0.65}\text{Sr}_{0.35}\text{TiO}_3$  is a good target composition for the optimization of the dielectric properties for room-temperature operation of BST devices. Finally, there is a need for controlling film stress and oxygen vacancies in thin-film BST for the realization of improved reproducibility in the growth processes.

#### ACKNOWLEDGMENTS

The authors thank Mohammad Fatemi for the use of his x-ray diffractometer and Jeff Mittereder for the use of his AFM. This work was supported by the Office of Naval Research and Defense Advanced Research Project Agency.

<sup>1</sup>V. K. Varadan, D. K. Ghodgaonkar, V. V. Varadan, J. F. Kelly, and P. Gilkerdas, *Microwave J.* **35**, 116 (1992).

- <sup>2</sup>J. F. Scott and C. A. Paz de Araujo, *Science* **246**, 1400 (1989).  
<sup>3</sup>E. J. Cukauskas, S. W. Kirchoefer, W. J. DeSisto, and J. M. Pond, *Appl. Phys. Lett.* **74**, 4034 (1999).  
<sup>4</sup>J. A. Thornton and A. S. Penfold, in *Thin Film Processes*, edited by J. L. Vossen and W. Kern (Academic, New York, 1978), p. 107.  
<sup>5</sup>J. Geerk, G. Linker, O. Meyer, F. Ratzel, J. Reiner, J. Remmel, T. Kroner, R. Henn, S. Massing, E. Brecht, B. Strehlau, R. Smithey, R. L. Wang, F. Wang, M. Siegel, C. Ritschel, and B. Rauschenbach, *Proc. SPIE* **1597**, 147 (1991).  
<sup>6</sup>Y. Fukuda, H. Haneda, I. Sakaguchi, K. Numata, K. Aoki, and A. Nishimura, *Jpn. J. Appl. Phys., Part 2* **36**, L1514 (1997).  
<sup>7</sup>L. Zhang, W. L. Zhong, Y. G. Wang, and P. L. Zhang, *Solid State Commun.* **104**, 263 (1997).  
<sup>8</sup>J. M. Pond, S. W. Kirchoefer, W. Chang, J. S. Horwitz, and D. B. Chrisey, *Integr. Ferroelectr.* **22**, 317 (1998).  
<sup>9</sup>S. S. Gevorgian, T. Martinsson, P. I. J. Linner, and E. L. Kollberg, *IEEE Trans. Microwave Theory Tech.* **44**, 896 (1996).  
<sup>10</sup>V. Balu, T. Chen, S. Katakam, J. Lee, B. White, S. Zafar, B. Jiang, P. Zurcher, R. E. Jones, and J. C. Lee, *Integr. Ferroelectr.* **21**, 155 (1998).  
<sup>11</sup>S. Lee, K. Kang, and S. Han, *Appl. Phys. Lett.* **75**, 1784 (1999).  
<sup>12</sup>J. D. Baniecki, R. B. Laibowitz, T. M. Shaw, P. R. Duncombe, D. A. Neumayer, D. E. Kotecki, H. Shen, and Q. Y. Ma, *Appl. Phys. Lett.* **72**, 498 (1998).  
<sup>13</sup>K. Ueki, A. Tokiwa, M. Kikuchi, T. Suzuki, M. Nagoshi, R. Suzuki, N. Kobayashi, and Y. Syono, *Advances in Superconductivity II* (Tsukuba, Japan, 1989), pp. 489–492.  
<sup>14</sup>L. Davis, Jr. and L. G. Rubin, *J. Appl. Phys.* **24**, 1194 (1953).  
<sup>15</sup>S. Zafar, R. E. Jones, B. Jiang, B. White, P. Chu, D. Taylor, and S. Gillespie, *Appl. Phys. Lett.* **73**, 175 (1998).  
<sup>16</sup>W. L. Warren, K. Vanheusden, D. Dimos, G. E. Pike, and B. A. Tuttle, *J. Am. Ceram. Soc.* **79**, 536 (1996).  
<sup>17</sup>R. Waser, T. Baiatu, and K. Hardtl, *J. Am. Ceram. Soc.* **73**, 1645 (1990).  
<sup>18</sup>S. Maruno, T. Kuroiwa, N. Mikami, K. Sato, S. Ohmura, M. Kaida, T. Yasue, and T. Koshikawa, *Appl. Phys. Lett.* **73**, 954 (1998).  
<sup>19</sup>C. S. Hwang, B. T. Lee, C. S. Kang, J. W. Kim, K. H. Lee, H. Cho, H. Horii, W. D. Kim, S. I. Lee, Y. B. Roh, and M. Y. Lee, *J. Appl. Phys.* **83**, 3703 (1998).  
<sup>20</sup>S. S. Kim and C. Park, *Appl. Phys. Lett.* **75**, 2554 (1999).